A Monte Carlo Study for Photoneutron Dose Estimations around the High-Energy Linacs

Mohammadi N[1], Miri-Hakimabad S H[1]*, Rafat-Motavalli L[1]

[1]Physics Department, Faculty of Sciences, Ferdowsi University of Mashhad, Iran

ABSTRACT

Background: High-energy linear accelerator (linac) is a valuable tool and the most commonly used device for external beam radiation treatments in cancer patients. In the linac head, high-energy photons with energies above the threshold of (γ,n) interaction produce photoneutrons. These photoneutrons deliver the extra dose to the patients undergoing radiation treatment and increase the risk of secondary cancer.

Objective: In this study, a simplified model of the linac head was simulated and photoneutron dose equivalent was calculated at the isocenter and maze in the sphere detector. In addition, the absorbed and equivalent dose of photoneutron were estimated in the some organs of the phantom.

Methods: The simulations were made using the Monte Carlo code. The ICRP reference adult male voxel phantom was used as the human body model for dosimetry calculations.

Results: The results of dose calculations at the isocenter and maze showed that photoneutron dose decreases as the function of distance from the isocenter and increases with increasing the distance from the entrance maze.

Conclusion: It is concluded that the simplified model of linac head is a useful and reliable method in dosimetry calculations. Calculations illustrated that the photoneutron dose is not negligible and duo to its harmful biological effects on body, it should be considered in the treatment plans.

Keywords

Linear accelerator, Monte Carlo, Photoneutron, Dosimetry, Phantom

Introduction

Nowadays, using medical linear accelerator operating over 10 MV has increased for cancer treatment at radiotherapy centers. Photon beams produced by these linacs have several advantages among the other radiotherapy treatments such as higher dose in depth, lower skin dose, reduced amount of scattered dose on healthy tissues around the tumor and lower isodose curve [1,2]. According to the operating voltage of the linac, the maximum energy of photon ranges from 8 MeV to 25 MeV. Whereas, the required threshold energy for (γ,n) interactions in heavy materials is about 8 MeV (e.g. is 7.34 MeV for tungsten) [3,4].Therefore, the high-energy photons can collide with the high-Z nucleus of target, collimator, and flattening filter of linac head such as tungsten and lead and eventually photoneutrons will be produced. The level of additional and unwanted photoneutron doses in patients has increased concerns about developing further damages in

*Corresponding author: S H Miri-Hakimabad Physics Department, Faculty of Sciences, Ferdowsi University of Mashhad, Iran
E-mail: mirihakim@ferdowsi.um.ac.ir

normal tissues and increasing the risk of secondary cancers. These amounts of radiation dose can also cause damages in the personnel of radiotherapy center working in the maze of the treatment room. Considering the facts that a high intensity of photon flux needed to kill tumor cells and such intensity creates destructive effects in human body the estimation of received doses by the patients and staffs is essential.

In this work, MCNPX 2.4.0 Monte Carlo code was used for all simulations [5]. The simplified geometry of the linac head was simulated and the photoneutron spectra and the photoneutron dose equivalent were calculated at the isocenter and the maze of the treatment room for a linac operating in 15,18,20, and 25 MV. To assess the photoneutron dose in the patients, the ICRP reference adult male voxel phantom was used and the photoneutron absorbed doses (sum of the absorbed doses of photoneutrons and photons from photoneutron interactions with the body composition) were calculated in the organs of this realistic voxel phantom in a brain, stomach, pancreas, and prostate treatments with a 15, 18, 20, and 25 MV accelerators. Furthermore, the photoneutron equivalent dose in the relevant organs was calculated in order to provide quantitative criteria for comparison.

Materials and Methods

Photoneutron source

The photoneutrons produced in high-energy accelerator can be classified in two groups: the first group has a Maxwellian energy distribution, which are called evaporation neutrons. When the energy of incident photon distribute among all the nucleons of the nucleus, a neutron which is close to the nucleus surface acquires enough energy to emerge as an evaporation neutron. These neutrons have isotropic angular distributions. The second group produced through direct interaction between a photon and a neutron in the nucleus. In this case, the photon gives all its energy to the neutron. These neutrons are mostly emitted in the direction of the in-coming photon and are known as knock-on neutrons [6].In addition, their energies are greater than evaporation neutrons. Nevertheless, the evaporation neutrons constitute the larger portion of the photoneutrons. To describe the photoneutron spectra the following equation was derived:

$$\frac{dN}{dE} = \alpha \frac{E}{T^2} e^{\frac{-E}{T}} + \beta \frac{\ln\left|E_{max} / E + S_n\right|}{\int_0^{E_{max}-S_n} \ln\left|E_{max} / E + S_n\right| dE} \quad (1)$$

where dN/dE is the amount of the neutrons with energy between E and E+dE. The first part is corresponding to the evaporation neutrons in which α is the fraction of evaporation neutrons, and T is the target nuclear temperature in MeV. In the second part, β is the fraction of the knock-on neutrons, E_{max} is the maximum energy of accelerated electrons and S_n is the separation energy of neutrons in the target nucleus. For tungsten target, α=0.8929, β=0.1071, T=0.5 MeV, and S_n=7.34 MeV.

MCNP simulations

The detailed geometry of linac is not always available. So, to confront this limitation, a simplified model of linac was simulated by Monte Carlo N-Particle (MCNP) to study neutron transport around the linac. This approach was used by other authors successfully [6-9]. In the linac head, the main source of photoneutrons is the reactions between photons and tungsten. Therefore, the simplified geometry of the head was simulated as 10 cm-thick spherical shell of tungsten with an air conical aperture. The point-like source of the photoneutron with spectra given by eq.1 was located in the center shell. The average photoneutron energies of these spectra were 1.15, 1.25, 1.31, and 1.46 MeV for 15, 18, 20, and 25 MV, respectively. In order to simulate the different radiation field sizes a suitable angle of cone was considered. The used photoneutron spectrum and simplified model of the simulated head were shown in figures1 and 2.

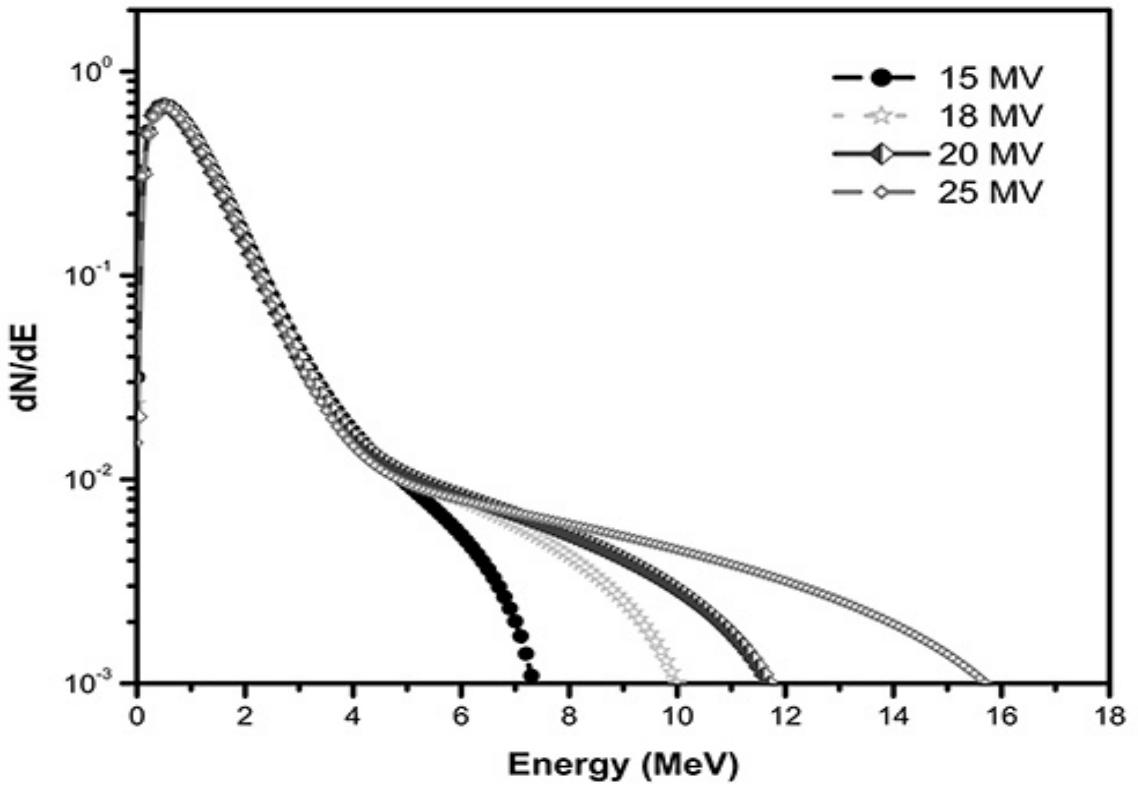

Figure 1: The photoneutron spectra derived from Eq. 1

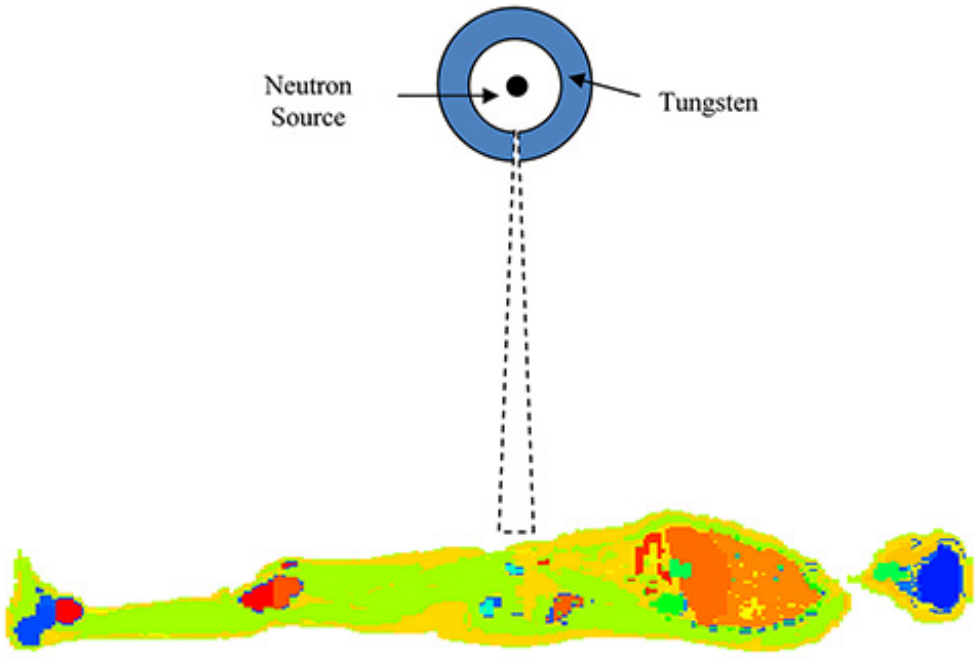

Figure 2: The simplified model of linac head and voxel phantom in MCNPX simulation

Simulation of the treatment room was based on Imam Reza hospital of Mashhad city in Iran. The thicknesses of the walls of treatment room and maze were considered 140 cm and 165 cm, respectively, which were made of standard concrete with a density of 2.23 $gr.cm^{-3}$. The isocenter was located at a height of 114 cm from the floor and the distance between the source and the isocenter was about 100 cm. The schematic view of the treatment room was shown in the figure 3.

To evaluate the photoneutron dose equivalent and photoneutron spectrum at the different distances from isocenter and the maze of the treatment room, the sphere with a diameter of 10 cm was simulated as a detector and was placed at the isocenter. Because of the body shape effects on the dose distribution, the sphere detector is not an adequate implement for estimation the received dose by patients. So, in the next step the voxel phantom was used and calculations were made for human body.

The absorbed dose in the organs and tissues due to photoneutrons produced in the clinical linacs cannot be measured directly but it can be calculated by using Monte Carlo simulation, which considers detailed and accurate model of the human body. To represent an accurate model of the human body with detailed internal structures, voxel phantoms were used which are based on the computed tomography (CT) or magnetic resonance imaging (MRI) images of real persons. Each voxel of this 3-D model of human body is characterized with its index and the constituent material.

To calculate the photoneutron dose in body organs, we used the ICRP reference adult male voxel phantom that has the height and the mass of 176 cm of 73 kg, respectively [10], and built of 254×127×222 voxels with dimensions of $0.2137\times0.2137\times0.8\ cm^3$.

Estimation of the photoneutron spectra and dose equivalent in the sphere detectors were done using the volumetric flux (F4 tally card), with flux-to-dose rate conversion factors reported by the NCRP38 [11]. The F6 tally and mean radiation weight factor of ICRP 103 were used for dose calculations in the voxel phantom [12]. S(α,β) treatment was used to account thermal neutron scattering in concrete and soft tissue. According to the thicknesses of the walls, the variance reduction method (Russian-Roulette) was considered in the MCNP input file. Ultimately, the statistical errors in all the calculations were less than 3%.

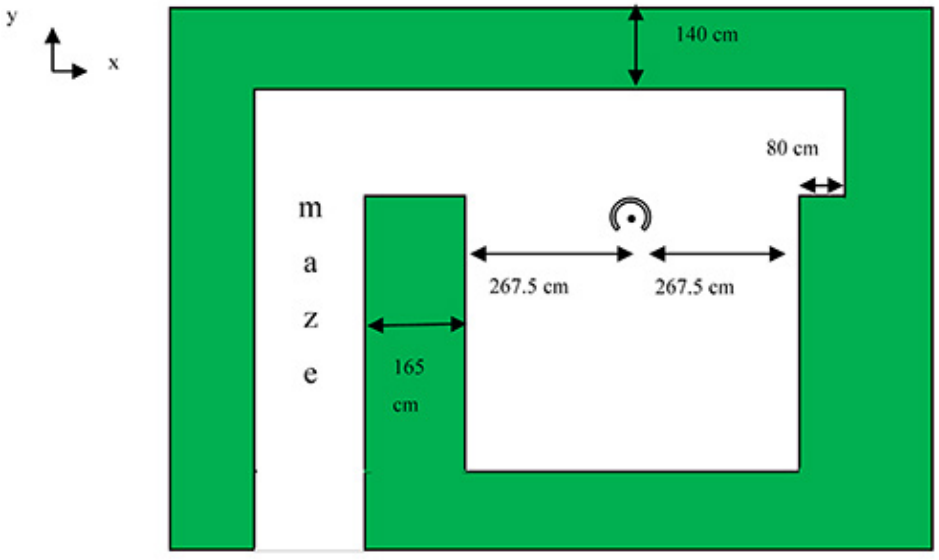

Figure 3: The x-y plan of simulated treatment room

In MCNPX, the tally results are reported per source particle. Therefore, to obtain neutron doses in each treatment, normalization factors were used to calculate the dose values per 1 Gy photon absorbed dose at the isocenter.

Although the strength of produced photoneutrons depend on the structure of the linac head, but their amounts are not differing significantly between the various types of linacs. So, the photoneutron strength per Gy (Q) measured by the other researchers for linacs operating in 15,18,20, and 25 MV, were used for calculations. These data were listed in table1. Since the MCNP outs are per incident neutron, all results were multiplied by the related Q.

Results and Discussion

Sphere detector

The fluences of photoneutrons in the spheres containing air and soft tissue at the isocenter (for 15 MV) were displayed in figures 4 and 5, respectively. There are two peaks in the spectrum: first one at energy of 0.5 MeV is due to direct neutrons which move directly from the head to the detectors and the second one at energy of 10^{-7} MeV is related to thermal neutrons produced by scattering from head's components and walls of treatment room. The results of our calculations for determining photoneutron spectra in air were in good

Table 1: The measured photoneutron strength (n /Gy) used in the calculations

Manufacturer	Model	Nominal MV	Q (n /Gy)	Study
Siemens	MD	15	0.2×10^{12}	Followill et al. (2003)[13]
Siemens	KD	18	0.88×10^{12}	Followill et al. (2003)[13]
Siemens	KD	20	0.92×10^{12}	McCall (1987)[14]
GE	Saturne 43	25	2.4×10^{12}	Fenn and McGinley (1995)[15]

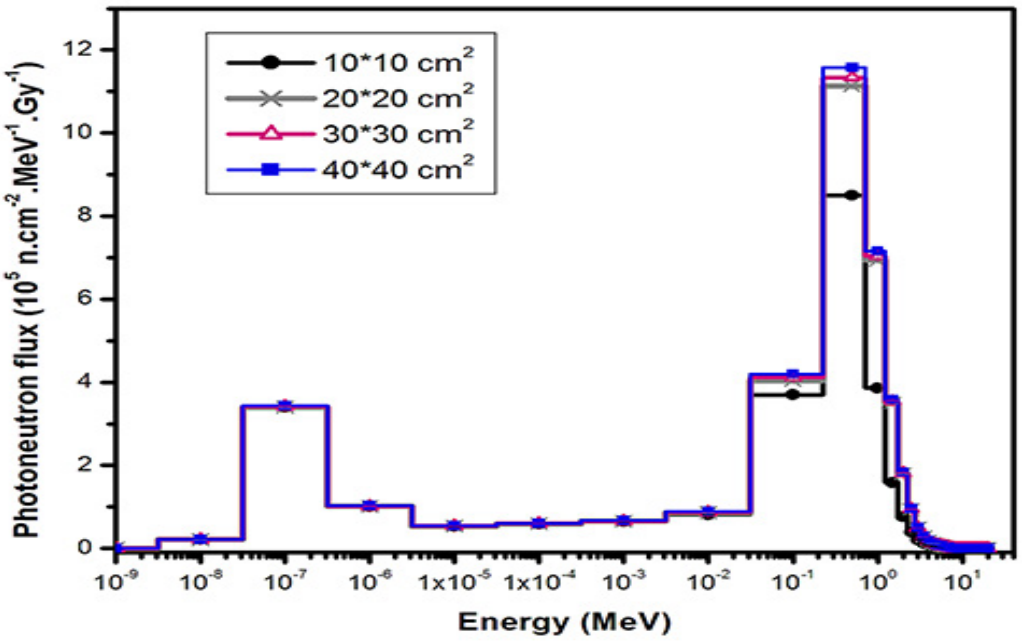

Figure 4: Photoneutron spectra at the isocenter (air) for 15 MV accelerator

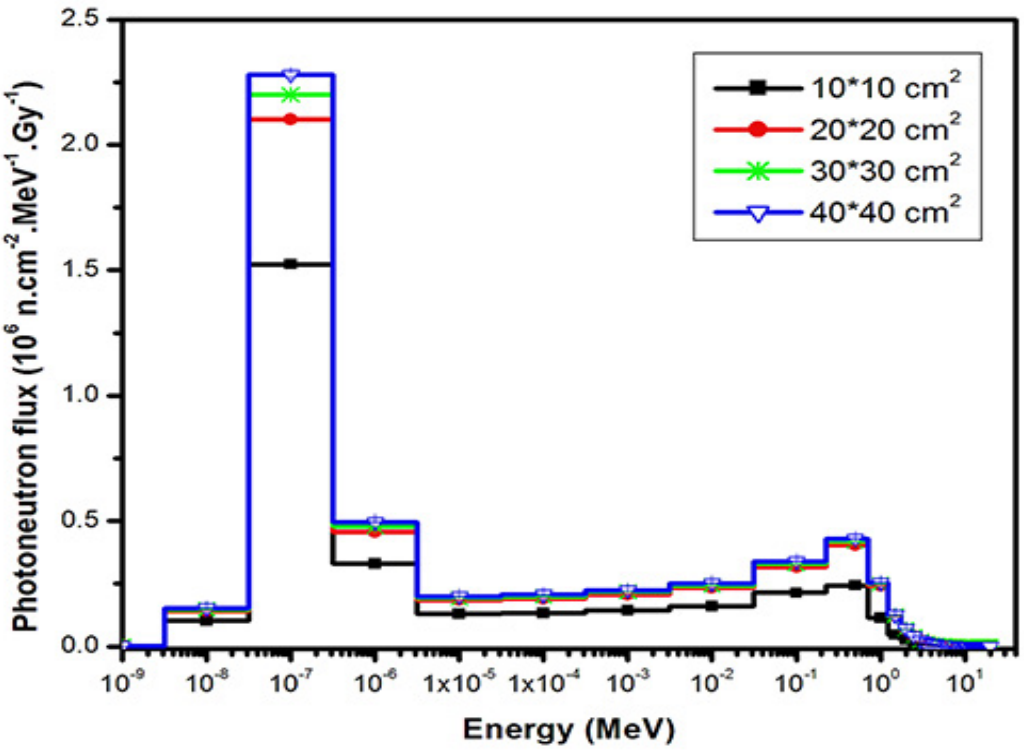

Figure 5: Photoneutron spectra at the isocenter (soft tissue) for 15 MV accelerator

agreements with spectra reported by the other researchers [16-18].

According to the figure 4, the dimensions of irradiation field does not affect the thermal neutron fluence in the air detectors significantly. So that, the frequency of thermal neutrons were increased less than of 2% for 40×40 cm^2 field size with respect to that of 10×10 cm^2 field size.

However, it should be noted that the rate of increase in neutron frequency in the energy of about 0.5 MeV is greater. So that, the 20×20 cm^2 field size increased the direct neutrons flux about 30% rather than 10×10 cm^2 field size. This increasing for 30×30 cm^2 and 40×40 cm^2 field sizes were about 33% and 35%, respectively. This means that the rate of increase in neutron fluence at larger irradiation fields was almost the same. Because of the importance of knowing the incident neutron flux on patients, the neutron spectrum was calculated in the soft tissue detectors.

Figure 5 illustrated the photoneutron flux in a spherical detector containing soft tissue. In this figure, two peaks were seen similar to air detectors. However, the peak corresponding to thermal neutrons was larger than theother peak, and a substantial reduction in the direct neutron peak was observed. These changes occur as fast neutrons lose their energies and rapidly become thermalized, primarily because they have relatively large cross sections for elastic scattering with hydrogen.

At irradiation fields of 20×20 cm^2, 30×30 cm^2, and 40×40 cm^2 thermal neutron fluence increase 38%, 45%, and 50% compared to that of 10×10 cm^2, respectively. While the rate of increase for fast neutrons at irradiation fields of 20×20 cm^2, 30×30 cm^2, and 40×40 cm^2 were 66%, 72%, and 76%, more than that of the irradiation fields of 10×10 cm^2,separately. These significant discrepancies between irradiation field of 10×10cm^2 and the larger ones are due to the size of spherical detector (radius of 10 cm). The photoneutron dose equivalent in the air as a function of distance from the isocenter for different field sizes and energy of 15 MV, was shown in the figure 6. For

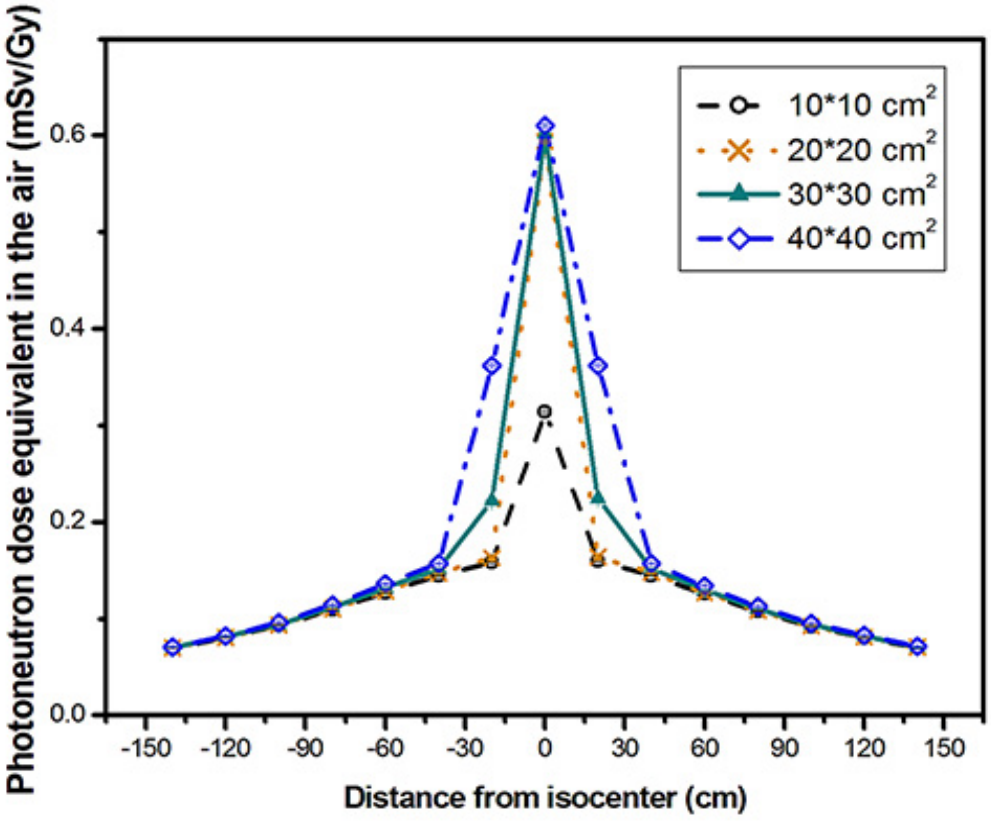

Figure 6: Photoneutron dose equivalent at different distances from the isocenter for 15 MV accelerator

all irradiation field sizes the amount of dose equivalent at the isocenter was larger than other positions. In addition, by dose equivalent at isocenter of larger field size were more than dose equivalent at irradiation field of 10×10 cm^2, so that this quantity at field size of 20×20cm^2, 30×30 cm^2, and 40×40 cm^2 was 47%, 48%, and 48.5%, higher than at 10×10 cm^2, respectively. The difference between dose equivalent of field sizes of 10×10 cm^2 and 20×20 cm^2 were considerable but the effect of field size of 20×20 cm^2 and 40×40 cm^2 on dose was almost the same. By increasing the distance from the isocenter(at 20 cm away from isocenter), a sharp drop was seen in the dose equivalent rate and for greater distances this reduction occurred with smoother slop. In the field size of 10×10 cm^2 the amount of dose reduction at 20 cm away from the isocenter was 50%, while dose equivalent at distances of 40 cm and 140 cm from isocenter were 9% and 56% less than that at 20 cm from the isocenter, respectively. This trend was similar for the other irradiation field sizes so that the amount of dose reduction relative to isocenter at distance of 20 cm were 73%, 63%, and 41% at field size of 20×20 cm^2, 30×30 cm^2, and 40×40 cm^2, separately. To compare and validate the results with the other published data, a neutron strength of 1.2×10^{12} n/Gy for 18 MV linac was used as Zabihzadeh et.al [19] and then the results compared by those of Sohrabi [20]. Table 2 indicates the results of this study and the corresponding values measured by Sohrabi et.al for 18 MV. Comparisons confirm that there is a good agreement between the outcomes of these two studies.

Dose equivalent was also calculated for 18, 20, and 25 MV at the different distance from the isocenter. The results showed that the photoneutron dose equivalent decreases with increasing distance from the isocenter.

Table 2: Comparison between calculated photoneutron dose equivalent and measured data (in air)

	Neutron dose equivalent at isocenter (mSv/Gy)		Neutron dose equivalent at 20 cm from the isocenter (mSv/Gy)	
	10×10 cm^2	40×40 cm^2	10×10 cm^2	40×40 cm^2
Measurement	2.2	3.7	0.5	2.0
This work	1.9	3.7	0.9	2.2

In general, the results showed that the dose equivalent of photoneutron at the isocenter was maximum, which were about 0.61, 2.71, 2.85, and 7.53 mSv/Gy for 15, 18, 20, and 25 MV respectively (for a 40×40 cm^2 field size). Moreover, it was observed that by decreasing the field size the neutron dose equivalent reduces, so that this quantity for a 10×10 cm^2 field size decreases to 0.3, 139, 1.47, and 3.88 mSv/Gy at the isocenter. It should be noted that by increasing the distance from the isocenter, the dose equivalent decreases gradually and falls to 0.07 ,0.31 ,0.33 and 0.89 mSv/Gy at a distance of 140 cm away from the isocenter for 15, 18, 20 and 25 MV, respectively (for a 40×40 cm^2 field size).

In order to estimate the amount of dose received to patient at maze, photoneutron dose equivalent was also calculated at different points in the maze. According to our results, the dimensions of irradiation fields have no effect on the neutron dose equivalent in the maze, so photoneutron dose equivalent for just 40×40 cm^2 field size at air detector placed at different distances from the entrance were displayed figure 7. Given the results, the dose equivalent at the entrance of the maze was lower than at the other points in the maze. By increasing the distance from the entrance of treatment room, dose equivalent increased, so that at energy of 25 MV this value was 1100%, 180%, and 167% higher than at energies of 15 MV, 18 MV, and 20 MV, separately. It should be mentioned that these remarkable enhance-

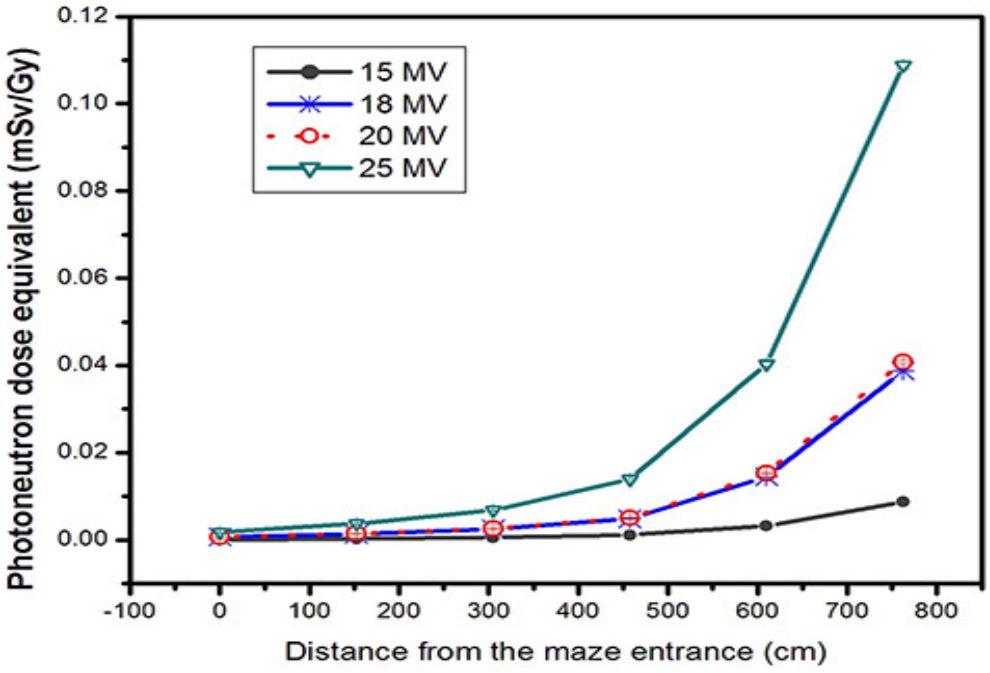

Figure 7: Photoneutron dose equivalent at different distances from the maze entrance

ment were due to the value of Q (the number of neutron produced at energy of 25MV per 1 Gy were 1100%, 180%, and 167% higher than at energies of 15 MV, 18 MV, and 20 MV, respectively).

Voxel phantom

Doses of the photoneutrons, produced from the linac head, is not taken into account in the treatment plans. While awareness of their amounts is very important to have a better estimation of secondary cancer risk, and also it can help in conducting the appropriate treatment plans for patients.

In this study, it was assumed that the patient was irradiated to treat the tumors in the brain, stomach, pancreas, and prostate. For this purpose, a simplified model of the linac head (as described above) was set in the front of these organs in the voxel phantom (AP geometry). So that, the distance between their center of masses and neutron source was 100 cm (i.e. the center of masses were located at the isocenter). Calculations were performed for 10×10 cm^2 irradiation field size and energy of 15, 18, 20, and 25 MV. This configuration is shown in the figure 2 for prostate treatment.

Photoneutron absorbed doses of adrenals, brain, gonads, liver, lungs, stomach, thyroid, gall bladder, heart, kidney, pancreas, prostate, spleen, thymus, and eye lens in the case that a simplified model of linac head was located in front of the brain were shown in the figure 8. Relative statistical uncertainties of these calculations were less than 3% except for the eye lenses, which was less than 10%.

According to the figure 8 and table 3, brain absorbed dose for 15, 18, 20, and 25 MV was 0.011, 0.052, 0.056, and 0.15 mGy/Gy, separately. Despite the fact that brain was the target,

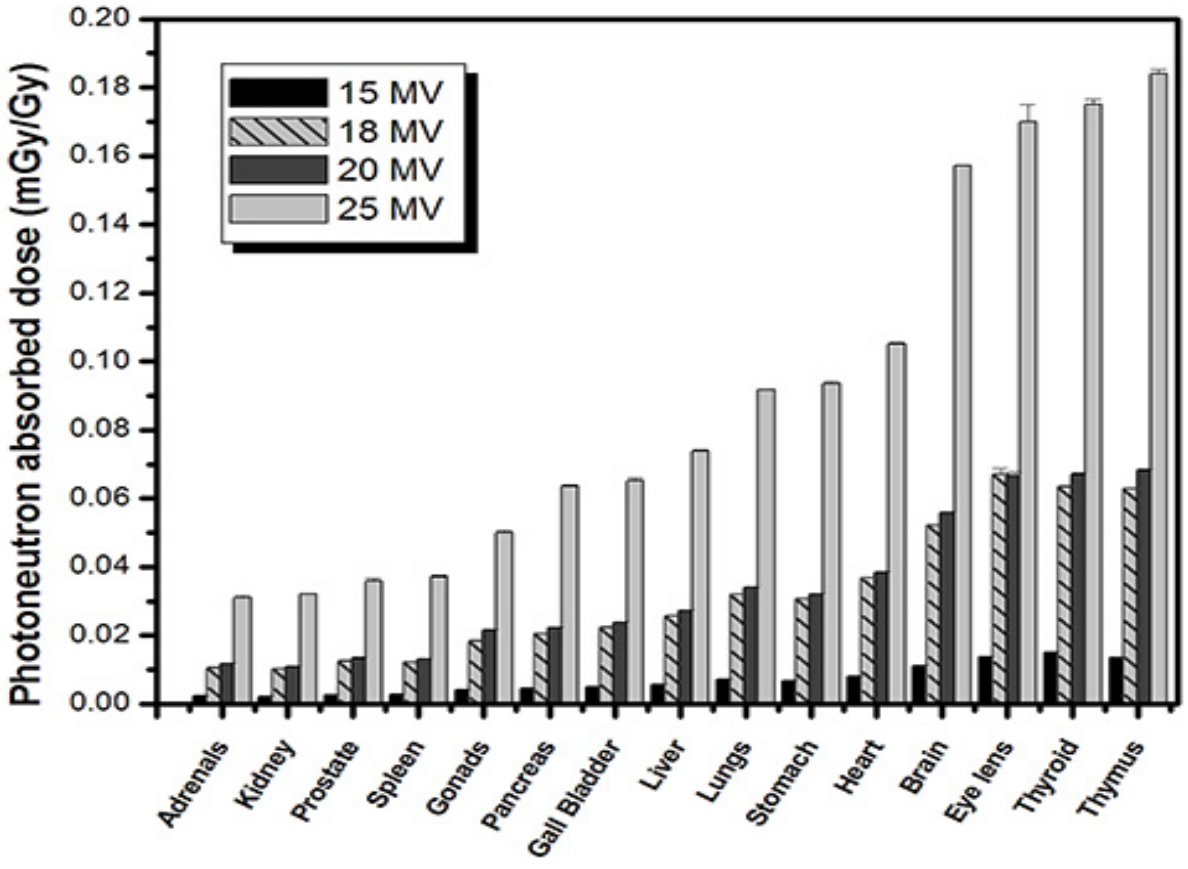

Figure 8: Photoneutron absorbed doses (mGy/Gy) in brain tumor treatment

Table 3: Absorbed dose and equivalent dose values of photoneutron in the brain tumor treatment

Organ	15 MV		18 MV		20 MV		25 MV	
	absorbed dose (10^{-3}mGy/Gy)	equivalent dose (10^{-2}mSv/Gy)	absorbed dose (10^{-2}mGy/Gy)	equivalent dose (10^{-2}mSv/Gy)	absorbed dose (10^{-2}mGy/Gy)	equivalent dose (10^{-2}mSv/Gy)	absorbed dose (10^{-2}mGy/Gy)	equivalent dose (10^{-2}mSv/Gy)
Adrenals	2.27	1.37	1.05	6.36	1.17	7.09	3.09	18.74
Kidney	2.25	1.36	1.02	6.18	1.09	6.61	3.21	19.46
Prostate	2.61	1.58	1.25	7.57	1.33	8.06	3.59	21.77
Spleen	2.75	1.67	1.23	7.45	1.3	7.88	3.71	22.49
Gonads	4.06	2.46	1.84	11.15	2.14	12.97	5	30.32
Pancreas	4.55	2.76	2.05	12.42	2.23	13.52	6.35	38.50
Gall Bladder	5.02	3.04	2.23	13.51	2.38	14.43	6.5	39.41
Liver	5.74	3.48	2.58	15.63	2.73	16.55	7.39	44.81
Lungs	7.08	4.29	3.2	19.38	3.4	20.61	9.17	55.60
Stomach	6.82	4.13	3.08	18.66	3.22	19.52	9.36	56.75
Heart	8.1	4.90	3.68	22.29	3.84	23.28	10.5	63.66
Brain	11.2	6.78	5.23	31.68	5.59	33.89	15.7	95.19
Eye lens	13.7	8.29	6.71	40.64	6.67	40.43	17	103.07
Thyroid	15.1	9.14	6.34	38.40	6.7	40.62	17.5	106.10
Thymus	13.6	8.23	6.28	38.04	6.82	41.34	18.4	111.56

the eye lenses, thyroid, and thymus received greater doses than brain, because they were more close to the body surface. The outcomes revealed that doses received by eye lenses, thyroid, and thymus were 21%, 34%, and 22% more than what brain received. In addition, the organs which were more distant from the brain, received less photoneutron doses than the closer ones. It should be mentioned that the great amounts of energy deposited in the thyroid and thymus were due to their proximity to the body surface, which cause them to be exposed to greater energies of photoneutrons. By increasing the energy, the dose increases, and this enhancement is very remarkable for 25 MV owing to its high neutron strength (2.4×10^{12} n/Gy). Calculations indicated that some normal tissues, which were not desired to be irradiated, also received high photoneutron equivalent dose. Because of these irreparable damages, concerns about neutron dose have increased.

Now suppose that the patient should receive photon dose of 50 Gy according to the prescribed treatment plan. Then the amount of absorbed dose of photoneutron in the sensitive organ such as thyroid for energies of 15, 18, 20 and 25 MV would be 0.755, 3.17, 3.35 and 8.75 mGy, respectively. In this case, the equivalent dose in the thyroid for mentioned energies will be 4.57, 19.2, 20.3, and 53.05 mSv, separately.

Due to the peak of incident neutron spectrum is in the range of 0.5-1 MeV and maximum W_R is in the same energy range, equivalent dose is high in the phantom organs. Therefore, the photoneutron dose should be considered in the designing of treatment plan. Because this high amount of dose equivalent causes to serious damage to healthy tissue certainly.

As expected, the maximum doses were delivered to stomach, pancreas, and prostate in stomach, pancreas, and prostate tumor treatments, respectively (tables 4-6). In these irradiations most of abdominal organs received extra doses that can increase the secondary

Table 4: Absorbed dose and equivalent dose values of photoneutron in the stomach tumor treatment

Organ	15 MV		18 MV		20 MV		25 MV	
	absorbed dose (10^{-3}mGy/Gy)	equivalent dose (10^{-2}mSv/Gy)	absorbed dose (10^{-2}mGy/Gy)	equivalent dose (10^{-2}mSv/Gy)	absorbed dose (10^{-2}mGy/Gy)	equivalent dose (10^{-2}mSv/Gy)	absorbed dose (10^{-2}mGy/Gy)	equivalent dose (10^{-2}mSv/Gy)
Adrenals	3.84	2.33	1.8	10.90	1.94	11.76	5.56	33.71
Kidney	3.71	2.25	1.72	10.42	1.87	11.34	5.42	32.86
Prostate	5.26	3.18	2.43	14.72	2.74	16.61	7.13	43.23
Spleen	4.94	2.99	2.35	14.23	2.58	15.64	7.34	44.50
Gonads	8.36	5.06	3.56	21.56	3.7	22.43	11.20	67.91
Pancreas	8.24	4.99	3.85	23.32	4.06	24.61	11.30	68.51
Gall Bladder	6.8	4.12	3.11	18.84	3.23	19.58	8.88	53.84
Liver	7.72	4.67	3.62	21.93	3.8	23.04	10.40	63.06
Lungs	6.78	4.11	3.11	18.84	3.29	19.94	9.05	54.87
Stomach	18.6	11.26	8.55	51.79	9.14	55.41	25.30	153.39
Heart	9.14	5.53	4.21	25.50	4.45	26.98	12.10	73.36
Brain	2.84	1.72	1.26	7.63	1.37	8.31	3.76	22.80
Eye lens	4.65	2.82	2.11	12.78	1.73	10.49	5.12	31.04
Thyroid	12.4	7.51	5.37	32.53	6.08	36.86	16.00	97.01
Thymus	12.3	7.45	5.68	34.40	6.14	37.22	15.60	94.58

Table 5: Absorbed dose and equivalent dose values of photoneutron in the prostate tumor treatment

Organ	15 MV		18 MV		20 MV		25 MV	
	absorbed dose (10^{-3}mGy/Gy)	equivalent dose (10^{-2}mSv/Gy)	absorbed dose (10^{-2}mGy/Gy)	equivalent dose (10^{-2}mSv/Gy)	absorbed dose (10^{-2}mGy/Gy)	equivalent dose (10^{-2}mSv/Gy)	absorbed dose (10^{-2}mGy/Gy)	equivalent dose (10^{-2}mSv/Gy)
Adrenals	2.55	1.54	1.13	6.84	1.25	7.58	3.43	20.80
Kidney	3.09	1.87	1.40	8.48	1.52	9.21	4.22	25.59
Prostate	16.90	10.23	7.94	48.09	8.51	51.59	23.70	143.69
Spleen	2.58	1.56	1.18	7.15	1.23	7.46	3.41	20.68
Gonads	15.70	9.51	6.78	41.07	7.34	44.50	19.10	115.80
Pancreas	5.85	3.54	2.69	16.29	2.84	17.22	7.66	46.44
Gall Bladder	5.98	3.62	2.73	16.54	2.92	17.70	7.94	48.14
Liver	5.58	3.38	2.55	15.45	2.74	16.61	7.61	46.14
Lungs	4.32	2.62	1.95	11.81	2.12	12.85	5.71	34.62
Stomach	7.00	4.24	3.20	19.38	3.45	20.91	9.36	56.75
Heart	5.36	3.25	2.45	14.84	2.61	15.82	7.01	42.50
Brain	1.80	1.09	0.83	5.05	0.91	5.53	2.59	15.70
Eye lens	3.34	2.02	1.46	8.84	1.50	9.09	3.17	19.22
Thyroid	8.58	5.19	3.82	23.14	3.96	24.01	10.60	64.27
Thymus	7.80	4.72	3.38	20.47	3.67	22.25	9.86	59.78

Table 6: Absorbed dose and equivalent dose values of photoneutron in the pancreas tumor treatment

Organ	15 MV		18 MV		20 MV		25 MV	
	absorbed dose (10^{-3}mGy/Gy)	equivalent dose (10^{-2}mSv/Gy)	absorbed dose (10^{-2}mGy/Gy)	equivalent dose (10^{-2}mSv/Gy)	absorbed dose (10^{-2}mGy/Gy)	equivalent dose (10^{-2}mSv/Gy)	absorbed dose (10^{-2}mGy/Gy)	equivalent dose (10^{-2}mSv/Gy)
Adrenals	3.74	2.26	1.75	10.60	1.98	12.00	5.43	32.92
Kidney	3.81	2.31	1.78	10.78	1.95	11.82	5.43	32.92
Prostate	5.92	3.58	2.50	15.14	2.86	17.34	7.46	45.23
Spleen	3.35	2.03	1.54	9.33	1.69	10.25	4.53	27.47
Gonads	9.06	5.49	4.02	24.35	4.36	26.43	11.30	68.51
Pancreas	13.00	7.87	6.06	36.71	6.64	40.25	18.30	110.95
Gall Bladder	9.76	5.91	4.57	27.68	4.87	29.52	13.60	82.46
Liver	9.30	5.63	4.22	25.56	4.54	27.52	12.30	74.58
Lungs	6.42	3.89	2.90	17.57	3.12	18.91	8.59	52.08
Stomach	12.50	7.57	5.63	34.10	6.15	37.28	16.50	100.04
Heart	8.00	4.84	3.63	21.99	3.86	23.40	10.50	63.66
Brain	2.78	1.68	1.30	7.87	1.37	8.31	3.72	22.55
Eye lens	4.63	2.80	2.46	14.90	2.31	14.00	7.18	43.53
Thyroid	12.40	7.51	5.44	32.95	5.45	33.04	14.60	88.52
Thymus	12.20	7.39	5.34	32.34	5.66	34.31	14.60	88.52

cancer risk in these regions.

Finally, the mesh tally was utilized to define the energy deposition distribution around the target volume of treatment. Then the stored energy in each voxel was divided by corresponding density, and the absorbed dose was calculated in the phantom. The size of each scoring cell of the mesh tally in the phantom was set to 0.2137 cm × 0.2137 cm × 0.8 cm as the same of voxel dimensions. Absorbed dose distribution around the prostate for energy of 15 MV is shown in the figure 9. According to the x-z view of this figure, the maximum absorbed dose was in the target volume, but in the surrounding tissue the value of absorbed dose was in the range of 14×10^{-3}-18×10^{-3} mGy/Gy. In other view(x-y plan), it was observed that the amount of absorbed dose in the skin and tissues close to the body surface was significant and ranged from14×10^{-3} to 24×10^{-3} mGy/

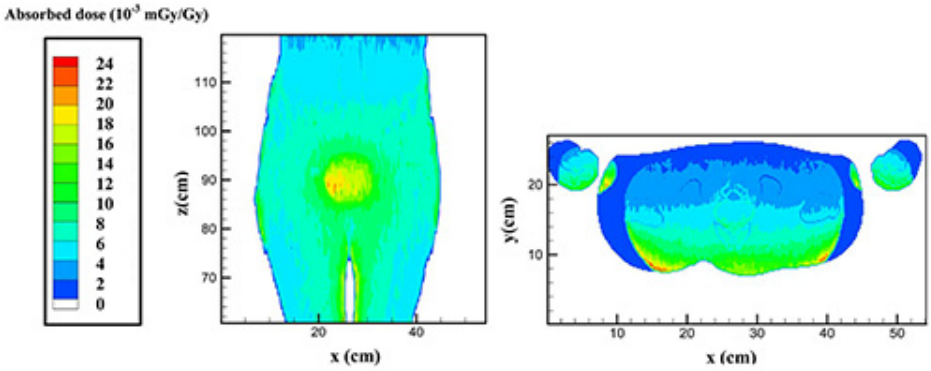

Figure 9: Photoneutron absorbed dose (mGy/Gy) distribution around the prostate in the prostate treatment for 15 MV accelerator

Gy. By increasing the depth and approaching to the back of body, absorbed dose decreased to 2×10^{-3} mGy/Gy. Unexpectedly, this reduction was not observed for two regions which were located in front of the hands and their absorbed doses were greater than the other positions of back of the body. This is due to the fact that hands acted as reflector and scattered the photoneutrons toward the body, so they caused enhancement in received doses in these regions. Therefore, to prevent this from happening it was suggested that patients were-placed in the arm raised position during the prostate treatment.

Conclusion

Unwanted neutrons are produced in the high-energy medical linear accelerators due to (γ,n) interaction in the heavy materials of the linac head. These photoneutrons deliver additional doses in the patients and even can lead to secondary cancer. Our calculations with MCNPX Monte Carlo code indicated that the photoneutron spectrum at the isocenter has two peaks in the thermal area and 0.5 MeV. The photoneutron dose equivalent had the maximum value at the isocenter, which was decreasing as the distance from the isocenter increases. Considering the results and good accordance obtained between calculations and measurements, it should be concluded that the simplified model of linac head is a useful and reliable method in dosimetry calculations. Moreover, using MCNPX code, photoneutron doses received in the whole anatomy of a realistic voxel male phantom undergoing a particular treatment, specifically brain, stomach, pancreas, and prostate treatments with 15, 18, 20, and 25 MV accelerators were calculated. It was also illustrated that the photoneutron dose is not negligible and duo to its harmful biological effects on body, it should be considered in the treatment plans.

Conflict of Interest

None

References

1. Vega-Carrillo HR, Hernandez-Almaraz B, Hernandez-Davila VM, Ortız-Hernande A. Neutron spectrum and doses in a 18 MV LINAC. *J Radioanal Nucl Chem.* 2010; **283**:261-265.
2. Hashemi SM, Hashemi-Malayeri B, Raisali G, *et al*. A study of the photoneutron dose equivalent resulting from a Saturne 20 medical linac using Monte Carlo method. *Nukleonika*. 2007;**52**(1):39-43.
3. Bedogni R, Pelliccioni M, Esposito A. A parametric model to describe neutron spectra around high-energy electron accelerators and its application in neutron spectrometry with Bonner Spheres. *Nucl Instrum Methods Phys Res A.* 2010; **615**:78-82.
4. Alfuraih A, Chin MPW, Spyrou NM. Measurements of the photonuclear neutron yield of 15 MV medical linear accelerator. *J Radioanal Nucl Chem.* 2008; **278**(3): 681-684.
5. Waters L. MCNPXTM user's manual version 2.4.0. 2002. Los Alamos National Laboratory Report LACP-02-408.
6. Facure A, Falcao RC, Silva AX, *et al*. A study of neutron spectra from medical linear accelerators. *Appl Radiat Isot*. 2005;**62**: 69-72.
7. Agosteo S, Para A F, Maggioni B. Neutron fluxes in radiotherapy rooms. *Med Phys*. 1993;**20**(2): 407-414.
8. Carinou E, Kamenopoulou V. Evaluation of neutron dose in the maze of medical accelerators. *Med Phys.* 1993;**26**(12): 2520-2525.
9. Ghiasi H, Mesbahi A. A Monte Carlo characterization of photoneutrons in the radiation therapy with high energy photons: a Comparison between simplified and full Monte Carlo models. *Iran J Radiat Res*. 2010;**8**(3): 187-193.
10. ICRP Publication 110. International Commission on Radiological Protection: Adult reference computational phantoms. 2009.
11. NCRP Report 38. National Council on Radiation Protection and Measurements: Protection against neutron radiation. 1971.
12. ICRP Publication 103. International Commission on Radiological Protection: Recommendations of the international commission on radiological protection. 2007.
13. Followill DS, Stovall MS, Kry SF, Ibbott GS. Neutron source strength measurements for Varian, Siemens, Elekta, and General Electric linear accelerators. *J Appl Clin Med Phys*. 2003;**4**:189-94.
14. McCall RC. Neutron yield of medical electron accelerators. SLAC-PUB 4480, Stanford CA, Stanford

Linear Accelerator Center. 1987.

15. Fenn JO, McGinley PH. Stray photoneutron fields produced by the GE Saturne accelerator. *Radiat Prot Manage.* 1995;**12**: 39-45.
16. Chu WH, Lan JH, Chao TC, *et al*. Neutron spectrometry and dosimetry around 15 MV linac. *Radiat Meas*. 2011;**46**:1741-1744.
17. Howell RM, Kry SF, Burgett E ,*et al*. Secondary neutron spectra from modern Varian, Siemens, and Elektalinacs with multileaf collimators. *Med Phys*. 2009;**36**(9): 4027-4038.
18. Amgarou K, Lacoste V, Martin A, *et al*. Neutron Spectrometry With a Passive Bonner Sphere System Around a Medical LINAC and Evaluation of the Associated Unfolding Uncertainties. *Nucl sci IEEE transactions on.* 2009;**56**(5): 2885-2895.
19. Zabihzadeh M, Ay MR, Allahverdi M, *et al*. Monte Carlo estimation of photoneutrons contamination from high-energy x-ray medical Accelerators in treatment room and maze: a Simplified model. *Radiat Prot Dosim.* 2009;**135**(1): 21-32.
20. Sohrabi M, Mostofizadeh A. Measurement of photoneutron dose in and out of high energy X-ray beam of a Saturne 20 medical linear accelerator by ECE polycarbonate detectors. *Radiat Meas*. 1999; **31**: 479-482.